
SEMI-SUPERVISED LEARNING OF MUTUALLY ACCELERATED MULTI-CONTRAST MRI SYNTHESIS WITHOUT FULLY-SAMPLED GROUND-TRUTHS

A PREPRINT

Mahmut Yurt^{1,2}, Salman Ul Hassan Dar^{1,2}, Berk Tınaz^{1,2,3}, Muzaffer Özbey^{1,2}, Tolga Çukur^{1,2,4}

¹ Department of Electrical and Electronics Engineering, Bilkent University, Ankara 06800, Turkey

² National Magnetic Resonance Research Center (UMRAM), Bilkent University, Ankara 06800, Turkey

³ Department of Electrical and Computer Engineering, University of Southern California, Los Angeles 90089, USA

⁴ Neuroscience Program, Bilkent University, Ankara 06800, Turkey

March 16, 2022

ABSTRACT

This study proposes a novel semi-supervised learning framework for mutually accelerated multi-contrast MRI synthesis that recovers high-quality images without demanding large training sets of costly fully-sampled source or ground-truth target images. The proposed method presents a selective loss function expressed only on a subset of the acquired k-space coefficients and further leverages randomized sampling patterns across training subjects to effectively learn relationships among acquired and nonacquired k-space coefficients at all locations. Comprehensive experiments performed on multi-contrast brain images clearly demonstrate that the proposed method maintains equivalent performance to the gold-standard method based on fully-supervised training while alleviating undesirable reliance of the current synthesis methods on large-scale fully-sampled MRI acquisitions.

Keywords magnetic resonance imaging, MRI, multi-contrast MRI, accelerated MRI, generative adversarial networks, image synthesis, semi-supervision, semi-supervised learning, selective loss

1 Introduction

Magnetic resonance imaging (MRI) is a preferred modality in clinical neuroimaging due to its excellent soft-tissue contrast. Its unique ability to acquire images of the given anatomy under a diverse array of distinct tissue contrasts further empowers it to accumulate complementary diagnostic information across an exam session [1]. However, lengthy scan durations associated with such multi-contrast MRI exams often result in acquisition of an incomplete set of the desired contrasts [2]. In turn, synthesis of the missing contrasts from the available ones emerges as a potential solution to enhance subsequent radiological observations as well as image analysis tasks, including detection, registration,

and segmentation [3]. This powerful potential has lead to a growing interest in multi-contrast MRI synthesis methods.

Recent studies have proposed adopting deep network models to multi-contrast MRI synthesis, given their promise in many other computer vision [4–8] and medical imaging tasks [3, 9–20]. In a fully-supervised learning setup, these deep network models are trained to estimate images of the target contrast from the images of the source contrasts, using pixel-wise, adversarial, or perceptual losses. These supervised methods have yielded success in synthesizing realistic, high-quality MR images [3, 9–20]. However, they require relatively large training sets with fully-sampled acquisitions of the source and target contrasts, compilation of which often proves infeasible due to limitations induced by scan durations, patient motion, examination costs, and physical constraints [2]. Therefore, there is a dire need for methods with lower reliance on supervised frameworks with fully-sampled MRI acquisitions for both source and ground-truth target images to enhance the practicality of synthetic MRI, as demonstrated in many other tasks in medical image processing [21–30].

Here, we propose a novel semi-supervised synthesis model for mutually accelerated multi-contrast MRI, namely ssGAN, that can be trained using only undersampled ground-truth acquisitions of the target contrast. To do this, ssGAN presents a selective loss function measuring the network error only on the k-space coefficients collected via undersampling patterns of the target contrast. ssGAN further leverages randomized undersampling patterns across training subjects to enable effective learning of relationships between acquired and nonacquired k-space coefficients at all locations. ssGAN further reduces the need for fully-sampled data by allowing synthesis from undersampled source contrast acquisitions. Its model is based on popular generative adversarial networks, which have been demonstrated to generate high-quality, realistic images [6, 7]. Comprehensive experiments performed on T_1 - and T_2 -weighted brain images clearly demonstrate that the proposed method maintains equivalent performance to the gold-standard model based on fully-supervised training, while at the same time alleviating undesirable dependency on large-scale fully-sampled MRI acquisitions.

2 Methods

2.1 Supervised Generative Adversarial Networks for MR Image Synthesis

Generative adversarial networks (GANs) [6] are deep generative models consisted of two competing subnetworks: a generator (G) and a discriminator (D). G aims to map a random noise vector z to a sample closely resembling a target domain distribution, whereas D aims to distinguish between arbitrary fake and real samples of the same target domain [6]. These two subnetworks are simultaneously trained via an adversarial loss [6], which is formulated as follows:

$$L_{GAN} = -E_y[(D(y) - 1)^2] - E_z[D(G(z))^2] \quad (1)$$

where E denotes expectation, and y denotes an arbitrary real sample in the target domain. Upon convergence, G is expected to generate realistic target domain samples that D cannot tell apart from the real ones.

While the traditional GAN models synthesize target samples given an arbitrary noise vector, several studies have demonstrated the effectiveness of conditional GAN (cGAN) models in image-to-image translation tasks [7]. The adversarial loss in cGAN models is modified by conditioning both G and D with a source domain image x [7]:

$$L_{cGAN} = -E_{x,y}[(D(x,y) - 1)^2] - E_x[D(G(x))^2] \quad (2)$$

When spatially aligned source and target images are available, a pixel-wise loss function is further

added to ensure reliable recovery [31].

$$L_{cGAN} = -\mathbb{E}_{x,y}[(D(x,y) - 1)^2] - \mathbb{E}_x[D(G(x))^2] + \mathbb{E}_{x,y}[\|y - G(x)\|_1] \quad (3)$$

Several studies have proposed cGAN models to MRI that synthesize target contrast from source contrast images of the same anatomy [8, 9, 11, 19]. These models typically learn the synthesis in a fully-supervised learning setup via a comprehensive training dataset of fully-sampled source and target images. Although they have demonstrated a state-of-the-art performance for synthetic MRI, they are inherently limited due their undesirable reliance on fully-sampled source and ground-truth target images, acquisition of which might prove impractical due to limitations induced by scan durations, patient motion, examination costs, and physical constraints [2]. Therefore, there is a critical need for methods with lower reliance on supervised frameworks with fully-sampled MRI acquisitions for many practical applications [21–30].

2.2 Semi-Supervised Generative Adversarial Networks

Here, we propose a novel semi-supervised generative adversarial network model (ssGAN) for high-quality multi-contrast MRI synthesis that allows a training protocol using only undersampled ground-truth acquisitions of the target contrast (i.e., without fully-sampled ground-truths). To do this, ssGAN introduces a selective loss function expressed only on acquired k-space coefficients of the undersampled target ground-truths and further leverages randomized sampling patterns across training subjects to effectively learn relationships between acquired and nonacquired k-space coefficients at all locations. ssGAN additionally reduces data requirements by allowing synthesis from undersampled source contrast acquisitions, which empowers ssGAN to alleviate the undesirable dependence on the fully-sampled source and ground-truth target acquisitions, which may be infeasible to acquire due to prolonged scan durations, examination costs, or physical constraints. Further details of the ssGAN model are provided below:

ssGAN receives as input either fully-sampled or undersampled images of the source contrast, and learns to synthesize fully-sampled images of the target contrast. A generator G first produces images of the target contrast as follows:

$$G(x_\Lambda) = \hat{y} \quad (4)$$

where x_Λ denotes the input source contrast image acquired with the sampling pattern Λ , and \hat{y} denotes the synthesized target contrast image. Since ssGAN only considers undersampled target ground-truths, a novel selective semi-supervised framework is utilized here for the network loss, where the synthesized images are evaluated only on the acquired k-space indices of the undersampled target ground-truth. To do this, undersampled counterparts of the synthesized fully-sampled images are computed by performing a binary masking in the k-space domain:

$$\hat{k}_{y_\Omega} = M(\mathcal{F}(\hat{y}), \Omega) \quad (5)$$

where \mathcal{F} denotes the forward Fourier transform, Ω denotes the indices of the acquired k-space points for the target ground-truth image y_Ω , M is an operator performing a masking in the k-space domain given k-space data and a sampling pattern, and \hat{k}_{y_Ω} denotes the undersampled k-space data of the synthesized fully-sampled image. Then, an L_1 loss in the k-space domain is formulated on the acquired k-space coefficients as follows:

$$L_k = \mathbb{E}_{x_\Lambda, y_\Omega} [\|\hat{k}_{y_\Omega} - \mathcal{F}(y_\Omega)\|_1] \quad (6)$$

To enhance the accuracy of the synthesized images, an image domain loss is also incorporated to

the semi-supervised framework. To do this, inverse Fourier transform of the masked k-space data is computed:

$$\hat{y}_\Omega = \mathcal{F}^{-1}(\hat{k}_{y_\Omega}) \quad (7)$$

where \mathcal{F}^{-1} denotes the inverse Fourier transform, and \hat{y}_Ω denotes the undersampled counterpart of the synthesized fully-sampled image. Then, an L_1 loss in the image domain between the ground-truth and synthesized images is defined as follows:

$$L_i = \mathbb{E}_{x_\Lambda, y_\Omega} [||\hat{y}_\Omega - y_\Omega||_1] \quad (8)$$

The synthesis quality is further enhanced via an adversarial loss, which is shown to generate highly realistic and plausible images. The formulation of this adversarial loss is as follows:

$$L_{adv} = -\mathbb{E}_{x_\Lambda, y_\Omega} [(D(x_\Lambda, y_\Omega) - 1)^2] - \mathbb{E}_{x_\Lambda} [D(x_\Lambda, \hat{y}_\Omega)^2] \quad (9)$$

where D denotes the discriminator that distinguishes between undersampled ground-truth and synthesized images. The L_1 losses in the k-space and image domains and the adversarial loss are aggregated using weighing parameters, yielding the following joint loss for the proposed semi-supervised approach:

$$L_{ssGAN} = \lambda_k L_k + \lambda_i L_i + \lambda_{adv} L_{adv} \quad (10)$$

where λ_k denotes the relative weighing of the k-space L_1 loss, λ_i denotes the relative weighing of the image domain L_1 loss, and λ_{adv} denotes the relative weighing of the adversarial loss.

2.3 Dataset

The proposed ssGAN model was demonstrated on the public IXI dataset consisted of multi-contrast brain MR images of healthy subjects. T₁- and T₂-weighted images of 94 subjects were used, where 64 of the subjects were reserved for training, 10 for validation, and 20 for testing. For each subject, approximately 100 axial cross-sections containing artifact-free brain tissues were manually selected. Since the multi-contrast images within each same subject were spatially unregistered, T₂-weighted images were registered onto T₁-weighted images prior to demonstrations. The registration was performed via FSL [32] using affine transformation based on mutual information. The images were originally acquired using the following scan parameters:

- **T₁-weighted images:** TR = 9.81 ms, TE = 4.603 ms, flip angle = 8°, volume size = 256 × 256 × 150, spatial resolution = 0.94 × 0.94 × 1.2 mm³.
- **T₂-weighted images:** TR = 8178.34 ms, TE = 100 ms, flip angle = 90°, volume size = 256 × 256 × 150, spatial resolution = 0.94 × 0.94 × 1.2 mm³.

For demonstrations, the images were retrospectively undersampled via uniform random sampling patterns for various acceleration factors ($R = 2, 3, 4$). The sampling patterns were generated to be distinct for each subject with an always fully-sampled central 10 × 10 region.

2.4 Implementation Details

The architecture and hyperparameters of ssGAN were mainly adopted from a previous study [11], which demonstrated a successful synthesis performance in multi-contrast MRI with conditional GANs. The resulting architecture consisted of a generator with an encoder of 3 convolutional layers,

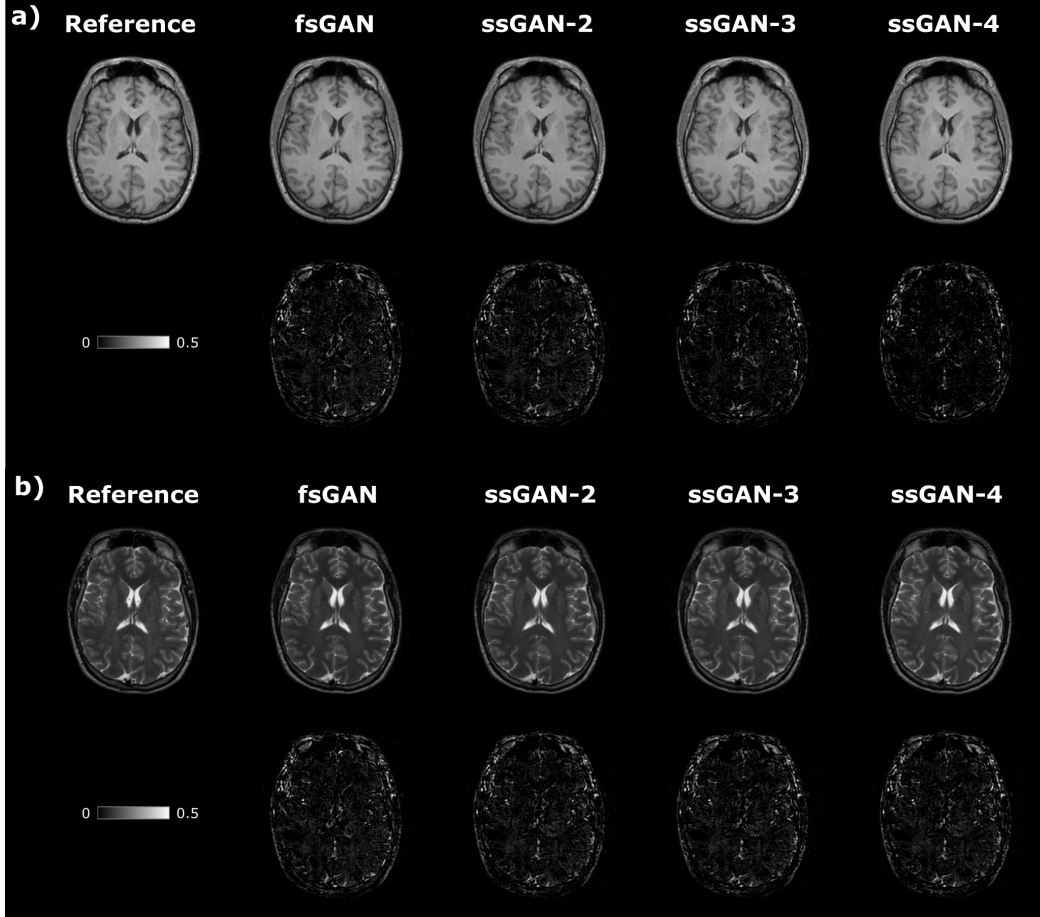


Figure 1: ssGAN was demonstrated on the IXI dataset against fsGAN for two distinct synthesis tasks: a) T₂-weighted image synthesis from fully-sampled T₁-weighted images, and b) T₁-weighted image synthesis from fully-sampled T₂-weighted images. Synthesized target images from ssGAN-2, ssGAN-3, ssGAN-4, and fsGAN are displayed along with fully-sampled reference target image.

a residual network of 9 ResNet blocks, and a decoder of 3 convolutional layers, and a discriminator with a convolutional network of 5 convolutional layers in series. ssGAN was trained for 100 epochs using the ADAM optimizer having gradient moments of $\beta_1 = 0.5$ and $\beta_2 = 0.999$. During the first 50 epochs, the learning rate was set to 0.0002, and during the remaining 50 epochs, the learning rate was linearly decayed to 0. The batch size was selected to be 1. The optimal relative weighing was determined to be 0.01 for the adversarial loss, 1 for the pixel-wise loss, and 30 for the k-space loss considering validation set performances.

2.5 Competing Method

The proposed ssGAN model was comparatively demonstrated against the gold-standard fully-supervised conditional GAN model, namely fsGAN, that is trained with fully-sampled target contrast images. This fsGAN model is learned using image domain L_1 , k-space domain L_1 and adversarial losses, as in ssGAN. For fsGAN, these losses are evaluated on all k-space coefficients. The architecture and hyperparameters of fsGAN were identical with those used in ssGAN.

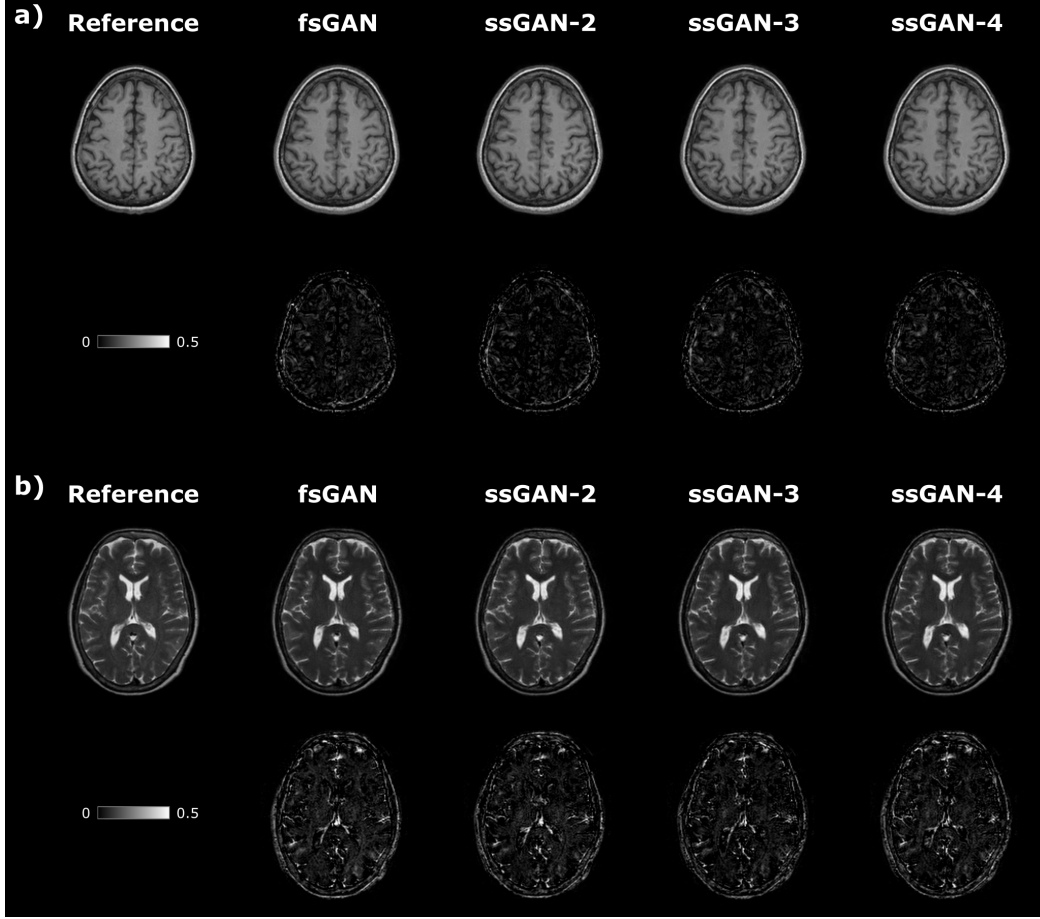


Figure 2: ssGAN was demonstrated on the IXI dataset against fsGAN for two distinct synthesis tasks: a) T_2 -weighted image synthesis from undersampled T_1 -weighted images ($R_{source} = 2$), and b) T_1 -weighted image synthesis from undersampled T_2 -weighted images ($R_{source} = 2$). Synthesized target images from ssGAN-2, ssGAN-3, ssGAN-4, and fsGAN are displayed along with fully-sampled reference target image.

2.6 Experiments

The proposed ssGAN model was demonstrated on the IXI dataset against the gold-standard fully-supervised fsGAN model for two distinct synthesis tasks: $T_1 \rightarrow T_2$ and $T_2 \rightarrow T_1$. In these synthesis tasks, fully-sampled target ground-truths were considered for the fsGAN model, whereas three separate acceleration ratios of the target contrast ground-truths ($R_{target} = 2, 3, 4$) were considered for the ssGAN model. Meanwhile, for both models, two separate cases were assumed for the source contrast images. In the first case, source contrast images were assumed to be fully-sampled, whereas in the second case, source contrast images were assumed to be undersampled with three distinct acceleration ratios ($R_{source} = 2, 3, 4$). The experiments were performed separately for each acceleration ratio R_{source} in the second case. Note that in all experiments, the training set was consisted of images of the source and target contrasts, and the test set was consisted of images of the source contrast only.

3 Results

We performed comprehensive experiments on the IXI dataset to demonstrate the proposed ssGAN model against the gold-standard fully-supervised fsGAN model. Two distinct synthesis tasks were demonstrated in the experiments: $T_1 \rightarrow T_2$ and $T_2 \rightarrow T_1$. In the demonstrations, a single fsGAN model was trained with fully-sampled target ground-truths, whereas three independent ssGAN models were trained with undersampled target ground-truths: ssGAN-2 was trained with $R_{\text{target}} = 2$, ssGAN-3 was trained with $R_{\text{target}} = 3$, and ssGAN-4 was trained with $R_{\text{target}} = 4$. We firstly considered that the source contrast input images are fully-sampled. The synthesis quality in terms of PSNR and SSIM measurements between the synthesized and fully-sampled reference images are reported in Table 1a for the methods under comparison. The reported measurements clearly indicate that all ssGAN models yield equivalent performance to fsGAN ($p > 0.5$, with Kruskal-Wallis). The equivalent performance of ssGAN is also visible in representative results displayed in Fig. 1a for T_1 -weighted image synthesis from T_2 -weighted images, and in Fig. 1b for T_2 -weighted image synthesis from T_1 -weighted images.

Table 1: Synthesis quality of ssGAN and fsGAN is reported in terms of PSNR (dB) and SSIM (%) measurements as mean \pm std. Four distinct acceleration ratios are considered for the source contrast images: a) fully-sampled source images, b) $R_{\text{source}} = 2$, c) $R_{\text{source}} = 3$, d) $R_{\text{source}} = 4$. Three separate models are reported for ssGAN based on the acceleration ratio of the target contrast ground-truths: ssGAN-2, ssGAN-3, and ssGAN-4.

		ssGAN-2	ssGAN-3	ssGAN-4	fsGAN
T1 → T2	PSNR	29.11	29.03	29.10	29.23
		±1.62	±1.63	±1.66	±1.70
	SSIM	93.41	93.42	93.33	93.63
		±1.68	±1.78	±1.71	±1.73
T2 → T1	PSNR	29.06	29.05	29.05	29.11
		±1.69	±1.62	±1.63	±1.76
	SSIM	94.27	94.25	94.23	94.53
		±1.86	±1.86	±1.83	±1.86

		ssGAN-2	ssGAN-3	ssGAN-4	fsGAN
T1 → T2	PSNR	27.44	27.30	27.27	27.59
		±1.60	±1.49	±1.56	±1.63
	SSIM	91.31	91.10	91.11	91.72
		±1.93	±1.93	±1.85	±1.94
T2 → T1	PSNR	27.88	27.86	27.80	28.11
		±1.46	±1.41	±1.41	±1.47
	SSIM	92.12	91.96	92.01	92.62
		±1.99	±1.94	±1.93	±1.88

		ssGAN-2	ssGAN-3	ssGAN-4	fsGAN
T1 → T2	PSNR	26.71	26.56	26.49	26.87
		±1.54	±1.53	±1.54	±1.58
	SSIM	90.26	89.86	89.95	90.79
		±1.91	±2.08	±2.00	±2.00
T2 → T1	PSNR	27.54	27.40	27.29	27.73
		±1.39	±1.40	±1.36	±1.37
	SSIM	91.33	90.81	90.98	91.79
		±1.96	±1.97	±1.95	±1.94

		ssGAN-2	ssGAN-3	ssGAN-4	fsGAN
T1 → T2	PSNR	26.04	25.91	25.81	26.16
		±1.57	±1.52	±1.58	±1.61
	SSIM	89.24	88.70	88.96	89.80
		±2.12	±2.17	±2.17	±2.10
T2 → T1	PSNR	27.18	27.00	26.93	27.31
		±1.36	±1.35	±1.38	±1.39
	SSIM	90.62	90.14	90.18	91.13
		±2.05	±2.07	±2.05	±2.06

Next, we considered that the source contrast images are undersampled with three distinct acceleration ratios ($R_{\text{source}} = 2, 3, 4$). We then compared synthesis quality of the proposed ssGAN and competing fsGAN models. The resulting measurements are reported in Table 1b-d in terms of PSNR and SSIM measurements between the synthesized and fully-sampled reference images. These results clearly suggest that all ssGAN models maintain equivalent performance to fsGAN ($p > 0.3$, with Kruskal-Wallis). The equivalent performance of ssGAN is also visible in representative results displayed in Fig. 2a for T_1 -weighted image synthesis from T_2 -weighted images, and in Fig. 2b for T_2 -weighted image synthesis from T_1 -weighted images. The overall results therefore strongly suggest that ssGAN synthesizes high-quality target contrast images without demanding large training sets of costly fully-sampled acquisitions of the target contrast.

4 Conclusion

In this study, we introduced a novel semi-supervised model for multi-contrast MRI synthesis based on conditional generative adversarial networks. The proposed method synthesizes high-quality target-contrast images without the need for large training sets containing costly fully-sampled acquisitions of the target or source contrasts. This performance leap is mediated via a novel selective k-space loss that is expressed only in the subset of available Fourier-domain coefficients of the target contrast, and via a randomized distribution of k-space sampling patterns across training subjects. The proposed method holds great promise for advancing the practical and clinical use of multi-contrast MRI synthesis.

5 Acknowledgments

This study was supported in part by a TUBITAK 1001 Research Grant (118E256), an EMBO Installation Grant (3028), a TUBA GEBIP 2015 fellowship, a BAGEP 2017 fellowship, and by NVIDIA under GPU grant.

References

- [1] J. E. Iglesias, E. Konukoglu, D. Zikic, B. Glocker, K. Van Leemput, and B. Fischl, “Is synthesizing MRI contrast useful for inter-modality analysis?,” in *Medical Image Computing and Computer-Assisted Intervention (MICCAI)*, pp. 631–638, Springer, 2013.
- [2] B. Thukral, “Problems and preferences in pediatric imaging,” *Indian Journal of Radiology and Imaging*, vol. 25, pp. 359–364, 11 2015.
- [3] B. E. Dewey, C. Zhao, J. C. Reinhold, A. Carass, K. C. Fitzgerald, E. S. Sotirchos, S. Saidha, J. Oh, D. L. Pham, P. A. Calabresi, P. C. van Zijl, and J. L. Prince, “DeepHarmony: A deep learning approach to contrast harmonization across scanner changes,” *Magnetic Resonance Imaging*, vol. 64, pp. 160 – 170, 2019.
- [4] Y. Choi, M. Choi, M. Kim, J.-W. Ha, S. Kim, and J. Choo, “StarGAN: Unified generative adversarial networks for multi-domain image-to-image translation,” in *Proceedings of the IEEE Conference on Computer Vision and Pattern Recognition*, 2018.
- [5] Y. Choi, Y. Uh, J. Yoo, and J.-W. Ha, “StarGAN v2: Diverse image synthesis for multiple domains,” in *Proceedings of the IEEE Conference on Computer Vision and Pattern Recognition*, 2020.
- [6] I. Goodfellow, J. Pouget-Abadie, M. Mirza, B. Xu, D. Warde-Farley, S. Ozair, A. Courville, and Y. Bengio, “Generative adversarial networks,” *Advances in Neural Information Processing Systems (NIPS)*, vol. 27, pp. 2672–2680, 06 2014.
- [7] M. Mirza and S. Osindero, “Conditional generative adversarial nets,” *arXiv preprint arXiv:1411.1784*, 11 2014.
- [8] D. Lee, J. Kim, W.-J. Moon, and J. C. Ye, “CollaGAN: Collaborative GAN for missing image data imputation,” in *Proceedings of the IEEE/CVF Conference on Computer Vision and Pattern Recognition (CVPR)*, June 2019.
- [9] H. Li, J. C. Paetzold, A. Sekuboyina, F. Kofler, J. Zhang, J. S. Kirschke, B. Wiestler, and B. Menze, “Diamondgan: Unified multi-modal generative adversarial networks for MRI sequences synthesis,” in *Medical Image Computing and Computer Assisted Intervention (MICCAI)*, pp. 795–803, Springer, 2019.
- [10] G. Litjens, T. Kooi, B. E. Bejnordi, A. A. A. Setio, F. Ciompi, M. Ghafoorian, J. A. Van Der Laak, B. Van Ginneken, and C. I. Sánchez, “A survey on deep learning in medical image analysis,” *Medical Image Analysis*, vol. 42, pp. 60–88, 2017.
- [11] S. U. H. Dar, M. Yurt, L. Karacan, A. Erdem, E. Erdem, and T. Cukur, “Image synthesis in multi-contrast MRI with conditional generative adversarial networks,” *IEEE Transactions on Medical Imaging*, vol. 38, pp. 2375–2388, 2019.
- [12] S. Olut, Y. H. Sahin, U. Demir, and G. Unal, “Generative adversarial training for MRA image synthesis using multi-contrast MRI,” in *PRedictive Intelligence in MEDicine (PRIME)*, pp. 147–154, Springer International Publishing, 2018.
- [13] A. Ben-Cohen, E. Klang, S. P. Raskin, S. Soffer, S. Ben-Haim, E. Konen, M. M. Amitai, and H. Greenspan, “Cross-modality synthesis from CT to PET using FCN and GAN networks for improved automated lesion detection,” *Engineering Applications of Artificial Intelligence*, vol. 78, pp. 186–194, 2019.
- [14] A. Chatsias, T. Joyce, M. Valerio Giuffrida, and S. Tsiftaris, “Multimodal MR synthesis via modality-invariant latent representation,” *IEEE Transactions on Medical Imaging*, vol. 37, pp. 803–814, 10 2017.
- [15] T. Joyce, A. Chatsias, and S. A. Tsiftaris, “Robust multi-modal MR image synthesis,” in *Medical Image Computing and Computer-Assisted Intervention (MICCAI)*, pp. 347–355, 2017.

- [16] W. Wei, E. Poirion, B. Bodini, S. Durrleman, O. Colliot, B. Stankoff, and N. Ayache, “FLAIR MR image synthesis by using 3D fully convolutional networks for multiple sclerosis,” in *ISMRM-ESMRMB - Joint Annual Meeting*, pp. 1–6, 06 2018.
- [17] D. Ravì, A. B. Szczotka, S. P. Pereira, and T. Vercauteren, “Adversarial training with cycle consistency for unsupervised super-resolution in endomicroscopy,” *Medical Image Analysis*, vol. 53, pp. 123–131, 2019.
- [18] K. Lei, M. Mardani, J. M. Pauly, and S. S. Vasanawala, “Wasserstein gans for mr imaging: from paired to unpaired training,” *IEEE Transactions on Medical Imaging*, pp. 1–1, 2020.
- [19] M. Yurt, S. U. H. Dar, A. Erdem, E. Erdem, and T. Cukur, “mustGAN: multi-stream generative adversarial networks for MR image synthesis,” *arXiv preprint arXiv:1909.11504*, 2019.
- [20] S. U. H. Dar, M. Yurt, M. E. Ildiz, M. Shahdloo, B. Tinaz, and T. Cukur, “Prior-guided image reconstruction for accelerated multi-contrast MRI via generative adversarial networks,” *IEEE Journal of Selected Topics in Signal Processing*, pp. 1–1, 2020.
- [21] S. A. H. Hosseini, C. Zhang, S. Weingärtner, S. Moeller, M. Stuber, K. Ugurbil, and M. Akçakaya, “Accelerated coronary MRI with sRAKI: a database-free self-consistent neural network k-space reconstruction for arbitrary undersampling,” *PLOS ONE*, vol. 15, pp. 1–13, 02 2020.
- [22] B. Yaman, S. A. H. Hosseini, S. Moeller, J. Ellermann, K. Ugurbil, and M. Akçakaya, “Self-supervised learning of physics-guided reconstruction neural networks without fully sampled reference data,” *Magnetic Resonance in Medicine*, vol. 84, no. 6, pp. 3172–3191, 2020.
- [23] M. Akçakaya, S. Moeller, S. Weingärtner, and K. Ugurbil, “Scan-specific robust artificial-neural-networks for k-space interpolation (RAKI) reconstruction: Database-free deep learning for fast imaging,” *Magnetic Resonance in Medicine*, vol. 81, no. 1, pp. 439–453, 2019.
- [24] E. K. Cole, J. M. Pauly, S. S. Vasanawala, and F. Ong, “Unsupervised MRI reconstruction with generative adversarial networks,” 2020.
- [25] G. Oh, J. E. Lee, and J. C. Ye, “Unsupervised MR motion artifact deep learning using outlier-rejecting bootstrap aggregation,” 2020.
- [26] S. Khan, J. Huh, and J. C. Ye, “Unsupervised deconvolution neural network for high quality ultrasound imaging,” in *2020 IEEE International Ultrasonics Symposium (IUS)*, pp. 1–4, 2020.
- [27] W. Burton, C. Myers, and P. Rullkoetter, “Semi-supervised learning for automatic segmentation of the knee from MRI with convolutional neural networks,” *Computer Methods and Programs in Biomedicine*, vol. 189, p. 105328, 2020.
- [28] H. E. Atlason, A. Love, S. Sigurdsson, V. Gudnason, and L. M. Ellingsen, “Segae: Unsupervised white matter lesion segmentation from brain MRIs using a CNN autoencoder,” *NeuroImage: Clinical*, vol. 24, p. 102085, 2019.
- [29] O. Beker, C. Liao, J. Cho, Z. Zhang, K. Setsompop, and B. Bilgic, “Scan-specific, parameter-free artifact reduction in k-space (spark),” 2019.
- [30] A. Jamaludin, T. Kadir, and A. Zisserman, “Self-supervised learning for spinal MRIs,” in *Deep Learning in Medical Image Analysis and Multimodal Learning for Clinical Decision Support* (M. J. Cardoso, T. Arbel, G. Carneiro, T. Syeda-Mahmood, J. M. R. Tavares, M. Moradi, A. Bradley, H. Greenspan, J. P. Papa, A. Madabhushi, J. C. Nascimento, J. S. Cardoso, V. Belagiannis, and Z. Lu, eds.), (Cham), pp. 294–302, Springer International Publishing, 2017.
- [31] P. Isola, J. Zhu, T. Zhou, and A. A. Efros, “Image-to-image translation with conditional adversarial networks,” in *2017 IEEE Conference on Computer Vision and Pattern Recognition (CVPR)*, pp. 5967–5976, July 2017.
- [32] M. Jenkinson and S. Smith, “A global optimisation method for robust affine registration of brain images,” *Medical Image Analysis*, vol. 5, pp. 143–156, 2001.